Mon. Not. R. Astron. Soc. **389,** 429–440 (2008) doi:10.1111/j.1365-2966.2008.13593.x

Seven young star clusters in the inner region of the Small Magellanic Cloud

Andrés E. Piatti,[1⋆] Doug Geisler,[2⋆] Ata Sarajedini,[3⋆] Carme Gallart[4⋆] and Marina Wischnjewsky[5]†

[1]*Instituto de Astronomía y Física del Espacio, CC 67, Suc. 28, 1428 Ciudad de Buenos Aires, Argentina*
[2]*Grupo de Astronomía, Departamento de Física, Universidad de Concepción, Casilla 160-C, Concepción, Chile*
[3]*Department of Astronomy, University of Florida, PO Box 112055, Gainesville, FL 32611, USA*
[4]*Instituto de Astrofísica de Canarias, Calle Vía Laćtea, E-38200 La Laguna, Tenerife, Spain*
[5]*Departamento de Astronomía, Universidad de Chile, Casilla 36-D, Santiago, Chile*

Accepted 2008 June 16. Received 2008 June 12; in original form 2008 May 9

ABSTRACT

We present CCD photometry in the Washington system C and T_1 passbands down to $T_1 \sim 22$ in the fields of L35, L45, L49, L50, L62, L63 and L85, seven poorly studied star clusters in the inner region of the Small Magellanic Cloud (SMC). We measured T_1 magnitudes and $C - T_1$ colours for a total of 114 826 stars distributed throughout cluster areas of 13.7×13.7 arcmin^2 each. Cluster radii were estimated from star counts distributed throughout the entire observed fields. The seven clusters are generally characterized by a relatively small angular size and by a high field star contamination. We performed an in-depth analysis of the field star contamination of the colour–magnitude diagrams (CMDs), and statistically cleaned the cluster CMDs. Based on the best fits of isochrones computed by the Padova group to the $(T_1, C - T_1)$ CMDs, we derive ages for the sample, assuming $Z = 0.004$, finding ages between 25 Myr and 1.2 Gyr. We then examined different relationships between positions in the SMC, age and metallicity of a larger sample of clusters including our previous work whose ages and metallicities are on the same scale used in this paper. We confirm previous results in the sense that the further a cluster is from the centre of the galaxy, the older and more metal poor it is, with some dispersion; although clusters associated with the Magellanic Bridge clearly do not obey the general trend. The number of clusters within $\sim 2^\circ$ of the SMC centre appears to have increased substantially after ∼2.5 Gyr ago, hinting at a burst.

Key words: techniques: photometric – galaxies: individual: SMC – Magellanic Clouds – galaxies: star clusters.

1 INTRODUCTION

Although the Small Magellanic Cloud (SMC) has a large number of relatively bright star clusters, surprisingly few have been studied in much detail. Indeed, due to the difficulties caused by the crowded star fields, the low cluster surface brightness with respect to that of the main body of the galaxy, the relatively high interstellar absorption etc., clusters located in the inner region of the SMC have only recently started to be the subject of detailed studies. The first sample of these clusters studied from modern CCD data was compiled by Pietrzyński & Udalski (1999), who presented determinations of reddenings and ages of clusters distributed within a 2.4 deg^2 region in the central part of the SMC. The photometric data used were taken from the *BVI* maps of the SMC and the catalogue of clusters in this galaxy obtained during the Optical Gravitational Lensing Experiment II (OGLE-II) microlensing survey (Pietrzyński et al. 1998). For 93 well populated SMC clusters their ages were derived with the standard procedure of isochrone fitting. They estimated the reddening values using the mean *I*-band magnitude of red clump (RC) stars in the cluster neighbourhood, ages using Bertelli et al.'s (1994) isochrones, adopting as a rule for the SMC a metallicity $Z = 0.004$, and an absolute distance modulus $(m - M) = 18.65$. de Oliveira et al. (2000) have also used the *BVI* OGLE-II data for estimating reddening and age for a sample of 91 clusters, 40 of them in common with Pietrzyński & Udalski (1999). de Oliveira et al. (2000) obtained from the data base *V*- and *I*-band colour–magnitude diagrams (CMDs) for these objects, using their coordinates and diameters to define a box extraction around each cluster. Guided by Digitized Sky Survey (DSS) images of each system

⋆E-mail: andres@iafe.uba.ar (AEP); dgeisler@astro-udec.cl (DG); ata@astro.ufl.edu (AS); carme@iac.es (CG)
†Deceased.

they selected representative field regions to measure stars and construct CMDs for comparison purposes. Ages and reddenings for the clusters were estimated by fitting the Padova isochrones (Bertelli, Bressan & Chiosi 1994), assuming $Z = 0.004$. They concluded that, despite the differences in the reddening method and distance modulus between their study and that by Pietrzyński & Udalski, there is a good overall agreement for the age determinations, as expected since they both used the same data base.

Rafelski & Zaritsky (2005) also presented age measurements for 195 star clusters in the SMC based on comparison of integrated colours measured from the Magellanic Cloud Photometric Survey (Zaritsky et al. 2002) with models of simple stellar populations. They compared the derived ages to those presented in the literature, including both via integrated colours or via isochrone fitting. Their ages are broadly correlated with those presented in the literature, although different patterns emerge when comparing to different data sets. Comparisons include papers by Pietrzyński & Udalski (1999) and de Oliveira et al. (2000), among others. More recently, Chiosi et al. (2006) studied 311 clusters in the context of a discussion of cluster and field star formation. They derived ages of the clusters from isochrone fitting to CMDs taken also from OGLE as well as their own imaging data. The fits were performed assuming a metallicity level of $Z = 0.008$, and an interstellar absorption $E(B - V) = 0.08$ whenever it was not possible to fit the zero-age main sequence (ZAMS). They also noted a broad correlation between their ages and those from Pietrzyński & Udalski and Rafelski & Zaritsky, respectively. From 204 clusters in common with Rafelski & Zaritsky, the dispersion around the 1:1 correlation line is $\sigma\ \log(t)/\log(t) = 0.4$. As can be seen, ages estimated from the mentioned surveys are very valuable from a global point of view, but some important differences arise from one study to another, particularly where the SMC metallicity and interstellar extinction values assumed are different.

Our group has been intensely involved in a long-term project aimed at obtaining ages and metallicities of SMC clusters. We have derived ages and metallicities for some 50 SMC clusters (Piatti et al. 2007c, and references therein), investigated the line-of-sight depth in the SMC (Crowl et al. 2001), identified new old clusters in the SMC (Piatti et al. 2007b), searched for age and metallicity gradients (Piatti et al. 2007c) and investigated in detail the age–metallicity relation (AMR; Piatti et al. 2007c). Our work has focused on obtaining ages and metallicities using the Washington photometric system. The Washington system is a particularly powerful photometric tool: Geisler & Sarajedini (1999) showed that their standard giant branch (SGB) technique in the system is three times more metallicity sensitive than the traditional $I, V - I$ technique. There are also good isochrones in the system (Girardi et al. 2002) and these indicate that the system is very competitive for obtaining ages as well. For these reasons, we decided to continue our program of enlarging the sample of well-studied SMC clusters with ages and metallicities placed on a homogenous scale that help us to improve our understanding of the SMC cluster formation and chemical evolution, by focusing in this case on clusters located in the inner region of the SMC.

Here, we present results on seven little-studied clusters (Lindsay numbers 35, 45, 49, 50, 62, 63 and 85) located in the inner part of the SMC, with the aim of adding them to our growing sample of well-studied clusters. The next section describes the observations and data reduction. Section 3 presents the procedure followed to estimate the cluster structural parameters, while Section 4 focuses on their CMDs including statistical field star subtraction, along with the estimation of the cluster properties. The analysis is continued in Section 5 together with a discussion of the results and their implications, which are summarized in Section 6.

2 OBSERVATIONS AND REDUCTIONS

The observations of the cluster sample were obtained with the Danish Faint Object Spectrograph and Camera (DFOSC) on the 1.54-m Danish Telescope at the European Southern Observatory (ESO) on La Silla, during the nights of 1999 November 5 and 6. We used the Washington C (Canterna 1976) and Kron–Cousins R filters in order to maintain consistency with our previous studies. The latter has a significantly higher throughput as compared with the standard Washington T_1 filter so that R magnitudes can be accurately transformed to yield T_1 magnitudes (Geisler 1996). The DFOSC imager has a field-of-view of 13.7×13.7 arcmin^2 with a plate scale of 0.42 arcsec pixel^{-1}. We obtained a series of bias and dome and sky flat-field exposures per filter to calibrate the CCD instrumental signature. Table 1 shows the log of the observations with filters, exposure times, airmasses and seeing estimates. All the data were

Table 1. Observation log of selected clusters.

Star cluster[a]	α_{2000} (h m s)	δ_{2000} (° ′ ″)	l (°)	b (°)	Date	Filter	Exposure (s)	Airmass	Seeing (arcsec)
K25, L35, SMC OGLE 45, RZ 54	0 48 01	−73 29 10	303.27	−43.64	1999 November 5	*C*	1800	1.39	2.2
						R	600	1.40	2.6
K30, L45, RZ 73	0 52 35	−72 11 35	302.81	−44.93	1999 November 5	*C*	1800	1.40	2.1
						R	600	1.43	1.6
NGC 299, K32, L49, ESO 51-SC5, RZ 85	0 53 25	−72 11 47	302.72	−44.93	1999 November 5	*C*	1800	1.40	2.1
						R	600	1.43	1.6
NGC 306, K33, L50, ESO 29-SC23, RZ 87	0 54 15	−72 14 29	302.63	−44.89	1999 November 5	*C*	1800	1.40	2.1
						R	600	1.43	1.6
IC 1612, K41, L62, ESO 29-SC28, SMC OGLE 120, RZ 116	1 00 01	−72 22 08	302.02	−44.74	1999 November 6	*C*	1800	1.42	1.8
						R	600	1.46	1.4
K42, L63, SMC OGLE 124, RZ 123	1 00 34	−72 21 56	301.96	−44.75	1999 November 6	*C*	1800	1.42	1.8
						R	600	1.46	1.4
NGC 419, K58, L85, ESO 29-SC33, SMC OGLE 159, RZ 174	1 08 19	−72 53 03	301.20	−44.19	1999 November 5	*C*	1800	1.46	2.3
						R	600	1.51	1.7

[a]Cluster identifications are from Lindsay (1958, L), Lauberts (1982, ESO), Kron (1956, K), Pietrzyński et al. (1998, SMC OGLE) and Rafelski & Zaritsky (2005, RZ).

taken under photometric conditions. On each photometric night, a large number (typically 20) of standard stars from the list of Geisler (1996) were also observed. Care was taken to cover a wide colour and airmass range for these standards in order to bracket and calibrate the program stars observed on these nights properly.

We applied bias subtraction to all the images and flat-fielding to both standard and programme field images, employing weighted combined signal-calibrator frames and standard observational techniques and tasks in IRAF.[1] The resulting processed images turned out to be satisfactorily flat. We then derived the instrumental magnitudes for the standard stars from aperture photometry using DAOPHOT/IRAF routines (Stetson, Davis & Crabtree 1990). We obtained the following mean transformation equations between instrumental and standard magnitudes through least-squares fit:

$$c = (1.682 \pm 0.016) + T_1 + (C - T_1) + (0.275 \pm 0.010)X_C - (0.150 \pm 0.012)(C - T_1), \quad (1)$$

$$r = (0.863 \pm 0.011) + T_1 + (0.097 \pm 0.004)X_{T_1} - (0.022 \pm 0.007)(C - T_1), \quad (2)$$

where X represents the effective airmass, and capital and lowercase letters stand for standard and instrumental magnitudes, respectively. The coefficients were derived through the IRAF routine FITPARAM, resulting in rms errors of 0.015 for c and 0.012 for r, indicating the nights were indeed photometric.

The stellar photometry was performed using the star finding and point spread function (PSF) fitting routines in the DAOPHOT/ALLSTAR suite of programs (Stetson et al. 1990). For each frame, a quadratically varying PSF was derived by fitting ∼100 stars, once the neighbours were eliminated by using a preliminary PSF. The preliminary PSF was obtained from 35 to 40 stars, which contained the brightest, least contaminated stars. Both groups of PSF stars were interactively selected. We then used the ALLSTAR program to apply the resulting PSF to the identified stellar objects and to create a subtracted image, which was used to find and measure magnitudes of additional fainter stars. This procedure was repeated three times for each frame. Finally, we computed aperture corrections from the comparison of PSF and aperture magnitudes using the neighbour-subtracted PSF star sample. The resulting aperture corrections were on average less than 0.01 mag (absolute value) for c and r images, respectively.

The resulting instrumental magnitudes were standardized using equations (1) and (2). We combined all the independent measurements using the stand-alone DAOMATCH and DAOMASTER programs kindly provided by Peter Stetson. The final information gathered for each cluster consists of a running number per star, the x and y coordinates, the measured T_1 magnitudes and $C - T_1$ colours and the observational errors $\sigma(T_1)$ and $\sigma(C - T_1)$, provided directly by ALLSTAR. We measured from around 20 000 to 35 000 stars, with an average of 30 000 stars, in each field. Tables 2–8 give this information for L35, L45, L49, L50, L62, L63 and L85, respectively. Only a portion of these tables is shown here, for guidance regarding their form and content; the whole content of Tables 2–8 is available in the online version of the journal. In Fig. 1 we plot – as an example – the CMD of all the measured stars in the field of L62. The remaining cluster fields have CMDs with similar appearance.

[1] IRAF is distributed by the National Optical Astronomy Observatories, which is operated by the Association of Universities for Research in Astronomy, Inc., under contract with the National Science Foundation.

Table 2. CCD CT_1 data of stars in the field of L35.

Star	X (pixel)	Y (pixel)	T_1 (mag)	$\sigma(T_1)$ (mag)	$C - T_1$ (mag)	$\sigma(C - T_1)$ (mag)
...	...	...	...	...	...	...
25	872.880	2.810	19.8690	0.0250	−0.0470	0.0280
26	1606.460	2.860	18.0740	0.0110	1.8700	0.0170
27	1097.100	3.040	20.8610	0.0400	0.1480	0.0520
...	...	...	...	...	...	...
...	...	...	...	...	...	...
...	...	...	...	...	...	...

Table 3. CCD CT_1 data of stars in the field of L45.

Star	X (pixel)	Y (pixel)	T_1 (mag)	$\sigma(T_1)$ (mag)	$C - T_1$ (mag)	$\sigma(C - T_1)$ (mag)
...	...	...	...	...	...	...
154	1912.090	9.150	20.5470	0.0360	−0.0650	0.0490
155	1857.930	9.180	18.6630	0.0070	−0.0470	0.0200
156	946.860	9.190	19.1320	0.0120	1.4400	0.0220
...	...	...	...	...	...	...
...	...	...	...	...	...	...
...	...	...	...	...	...	...

Table 4. CCD CT_1 data of stars in the field of L49.

Star	X (pixel)	Y (pixel)	T_1 (mag)	$\sigma(T_1)$ (mag)	$C - T_1$ (mag)	$\sigma(C - T_1)$ (mag)
...	...	...	...	...	...	...
319	1070.750	20.230	19.8140	0.0170	1.6050	0.0320
320	1697.050	20.290	19.5830	0.0190	−0.3600	0.0220
321	285.060	20.320	18.4870	0.0220	1.6760	0.0390
...	...	...	...	...	...	...
...	...	...	...	...	...	...
...	...	...	...	...	...	...

Table 5. CCD CT_1 data of stars in the field of L50.

Star	X (pixel)	Y (pixel)	T_1 (mag)	$\sigma(T_1)$ (mag)	$C - T_1$ (mag)	$\sigma(C - T_1)$ (mag)
...	...	...	...	...	...	...
534	625.350	34.060	19.9870	0.0330	−0.3390	0.0450
535	163.770	34.140	20.9450	0.0580	−0.2140	0.0650
536	1883.190	34.260	20.4070	0.0210	1.4270	0.0400
...	...	...	...	...	...	...
...	...	...	...	...	...	...
...	...	...	...	...	...	...

The CMDs clearly reveal the main SMC field features, characterized by the mixture of young and old stellar populations. The most obvious features are the long main sequence (MS) which extends approximately 6 mag in T_1, the populous and broad subgiant branch, indicator of the evolution of stars with ages (masses) within a non-negligible range, the RC and the red giant branch (RGB). The RC is somewhat elongated in T_1 and appears to be populated at brighter magnitudes by the so-called 'vertical red clump' structure (Zaritsky

Table 6. CCD CT_1 data of stars in the field of L62.

Star	X (pixel)	Y (pixel)	T_1 (mag)	$\sigma\,(T_1)$ (mag)	$C-T_1$ (mag)	$\sigma\,(C-T_1)$ (mag)
...	...	...	...	...	...	...
53	973.600	1.910	21.0790	0.0440	0.1380	0.0560
54	965.110	1.940	19.0230	0.0140	1.5130	0.0210
55	1627.470	1.970	18.9850	0.0270	1.4940	0.0360
...	...	...	...	...	...	...
...	...	...	...	...	...	...
...	...	...	...	...	...	...

Table 7. CCD CT_1 data of stars in the field of L63.

Star	X (pixel)	Y (pixel)	T_1 (mag)	$\sigma\,(T_1)$ (mag)	$C-T_1$ (mag)	$\sigma\,(C-T_1)$ (mag)
...	...	...	...	...	...	...
142	1119.620	6.810	17.1240	0.0110	2.3540	0.0160
143	1713.330	6.810	19.2620	0.0220	1.6280	0.0380
144	1053.140	6.860	21.0640	0.0490	0.0970	0.0560
...	...	...	...	...	...	...
...	...	...	...	...	...	...
...	...	...	...	...	...	...

Table 8. CCD CT_1 data of stars in the field of L85.

Star	X (pixel)	Y (pixel)	T_1 (mag)	$\sigma\,(T_1)$ (mag)	$C-T_1$ (mag)	$\sigma\,(C-T_1)$ (mag)
...	...	...	...	...	...	...
100	928.150	10.150	19.3350	0.0130	0.0700	0.0150
101	403.490	10.220	19.0320	0.0110	−0.3790	0.0190
102	1892.980	10.220	18.6190	0.0130	1.8240	0.0280
...	...	...	...	...	...	...
...	...	...	...	...	...	...
...	...	...	...	...	...	...

& Lin 1997; Gallart 1998; Ibata, Lewis & Beaulieu 1998). However, no clear evidence for the vertical structure stars seen in some Large Magellanic Cloud (LMC) fields (Piatti et al. 1999) exists.

We first examined the quality of our photometry in order to evaluate the influence of the photometric errors on the cluster fiducial characteristics in the CMDs. The T_1 magnitude and $C-T_1$ colour errors provided by DAOPHOT II are shown in Fig. 2. We only plotted the errors for stars measured in the field of L62, which are typical. The mean magnitude and colour errors for stars brighter than $T_1 = 19$ are in the range $\langle\sigma(T_1)\rangle = 0.015$–$0.030$ and $\langle\sigma(C-T_1)\rangle = 0.020$–$0.040$; for stars with $T_1 = 19$–21, $\langle\sigma(T_1)\rangle \leq 0.06$ and $\langle\sigma(C-T_1)\rangle \leq 0.08$ and for stars with $T_1 = 21$–22, $\langle\sigma(T_1)\rangle \leq 0.17$ and $\langle\sigma(C-T_1)\rangle \leq 0.23$. Thus, the quality of our photometry allowed us to detect and measure the turn-off (TO) for all of the clusters, which was used in our age estimates. Indeed, by using the relation between the TO R magnitude and age according to theoretical isochrones by Girardi et al. (2002) and by comparing it with our data, we concluded that we are able to define TOs for stellar populations as old as 5 ± 1 Gyr ($R \approx 22.0$) with an error of 0.20 in R. Slightly fainter TOs can be reached at the expense of larger errors.

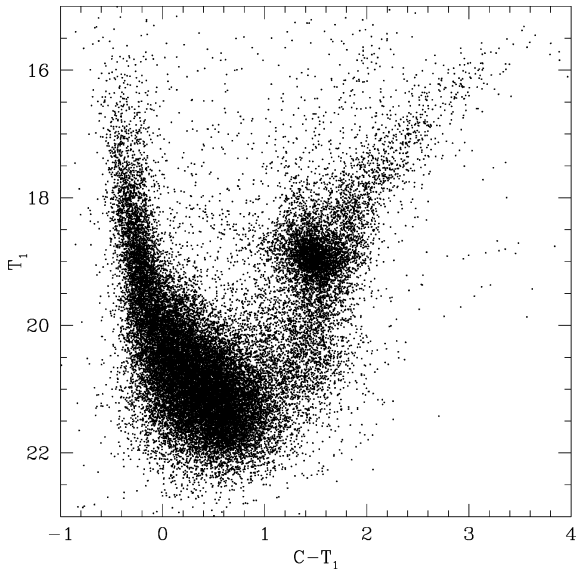

Figure 1. $(C-T_1, T_1)$ CMD for all the measured stars in the field of L62.

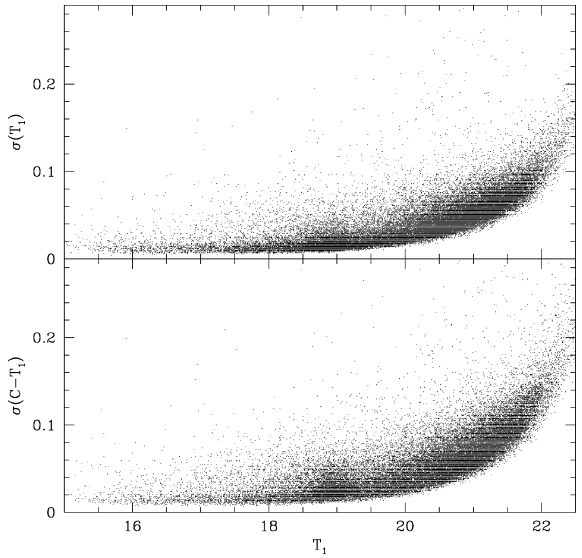

Figure 2. T_1 magnitude and $C-T_1$ colour photometric errors as a function of T_1 for stars measured in the field of L62.

3 CLUSTER STRUCTURAL PARAMETERS

The major challenge in obtaining reliable CMDs with the fiducial features of the clusters is to disentangle the stars belonging to the clusters, which are very small in angular extent, from those of their surrounding fields, which are close to the SMC centre and very populous. To do that, we built the cluster stellar density profiles, by first determining the location of their centres. This straightforward approach allows us not only to adopt optimum cluster radii, but also to obtain CMDs dominated by cluster stars. Some field star contamination is unavoidable, though. Obviously, the larger the ratio between the number of cluster stars to the number of field stars within each radius, the more robust this procedure.

We fitted Gaussian distributions to the star counts in the x and y directions of the fields – approximately parallel to the right ascension and the declination directions, respectively – to determine the coordinates of the cluster centres and their estimated uncertainties.

The number of stars projected along the x and y directions were counted within intervals 10-pixel wide, although we checked that using spatial bins from 20 to 50 pixel does not result in significant changes in the derived centres. The selected size of the box allowed us to sample statistically the stellar spatial distributions, particularly within the very small clusters, and to avoid spurious effects mainly caused by the presence of localized groups. The fit of a single Gaussian per cluster field was performed using the NGAUSSFIT routine in the STSDAS/IRAF package. The centre of the Gaussian, its amplitude and its full width at half-maximum (FWHM) acted as variables, while the constant and the linear terms were fixed to the value of the background level (the stellar field density assumed to be uniform) and to zero, respectively. We iterated the fitting procedure once on average, after eliminating a couple of discrepant points. The resulting values were compared with the cluster centres which were estimated by eye while looking at the cluster finding charts and were found to coincide within the errors. The cluster centres were finally determined with a typical standard deviation of ± 10 pixel ($\sim$4 arcsec). Note that the star counts were not weighted by luminosity, but the lack of very bright stars in these clusters implies that such weighting should not change the results significantly.

We then constructed the cluster radial profiles by computing the number of stars per unit area at a given radius r through the expression

$$(n_{r+5} - n_{r-5}) / \left[(m_{r+5} - m_{r-5}) 10^2\right], \quad (3)$$

where n_j and m_j represent the number of stars and boxes included in a circle of radius j, respectively. Note that this expression easily allows us to estimate the mean stellar density at a radius r without the need to trace a complete circle at that distance in the observed field. This is an important consideration in the sense that we have a stellar density profile which extends far away from the cluster centres. This allows us to estimate the background levels with higher precision. Since we define the cluster radius as the distance from the cluster's centre where the number of stars per unit area equals that of the background, it follows that the more precise the background level, the better estimated the cluster radius. On the other hand, it is also helpful to measure the FWHM of the stellar density profile and to determine the variation (in percentage) of the field star contamination in relation to the distance from the cluster's centre. In this way, we have a reference to perform optimum circular extractions including predominantly the cluster stellar population and to build reliably a cleaned cluster CMD.

The resulting density profiles expressed as number of stars per unit area in pixels are shown in Fig. 3. In that figure, we illustrate the region around the centres of the clusters up to 300-pixel radius. The background regions of the clusters were delimited by the observed field boundaries and by a circle of radius 300 pixel from the cluster's centres. The estimated background levels, the cluster radii ($r_{\rm cls}$) and the radii at the FWHM ($r_{\rm FWHM}$) are listed in Table 9. The adopted background levels and $r_{\rm FWHM}$'s are drawn in Fig. 3 with horizontal and vertical lines, respectively. With the sole exception of L85, cluster dimensions are very small: two/three of the cluster stellar populations are confined within a couple of tens of pixels, and the clusters fade into the background beyond $2r_{\rm FWHM}$. We also derived the statistical field star contamination percentage for the radial intervals $r < r_{\rm FWHM}$ and $r_{\rm FWHM} < r < r_{\rm cls}$, yielding the values quoted in columns 5 and 6 of Table 9. Note that the percentage of field stars is more than half of the total number of stars in the central cluster region ($r < r_{\rm FWHM}$), while only L85 stands out clearly over its surrounding field in a radial range from $r_{\rm FWHM}$ to $r_{\rm cls}$.

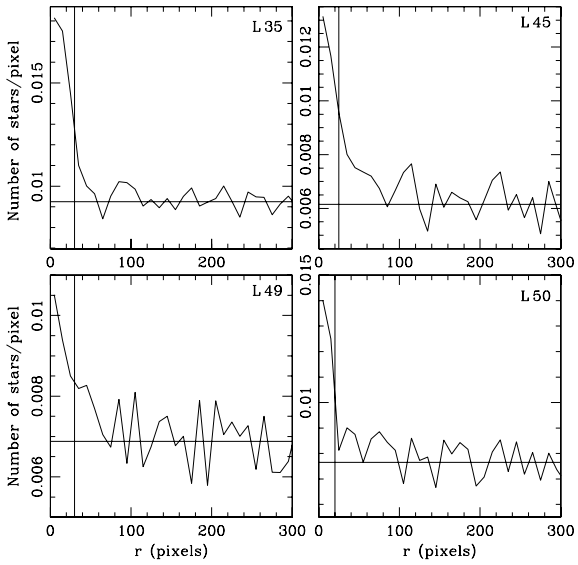

Figure 3. Stellar density profiles for the selected clusters: (a) L35 (upper left), L45 (upper right), L49 (bottom left) and L50 (bottom right); (b) L62 (upper left), L63 (upper right) and L85 (bottom). The horizontal lines correspond to the background levels far from the clusters, whereas the vertical lines indicate $r_{\rm FWHM}$.

It is worth mentioning that we did not succeed in our attempt to fit the well-known empirical model of King (1962) to the observed density profiles of our cluster sample, and hence, we could not estimate cluster core and tidal radii. As Piskunov et al. (2008) found, King models do not successfully work for star clusters having a small number of members, because that causes uncertainties in the observed density profiles. Furthermore, since the spatial boundaries of the observed clusters are not clearly defined and the proportion of field stars projected on the cluster area is relatively high, the King fits based on the inner area becomes less reliable. It can also lead to a significant bias in the resulting core radii. On the other hand, if we consider the behaviour of the density profile in the outer regions and even outside the cluster limits, the tidal radii would also be substantially uncertain. Tidal radii for old objects are usually found to be smaller than those for objects that are still dynamically young; so that the ratio of tidal to core radii can shed light on mass segregation. A similar trend is given by the ratio $r_{\rm cls}/r_{\rm FWHM}$. Note that this ratio is significantly smaller for L85, the oldest cluster of our sample.

4 CLUSTER PROPERTIES FROM THE CMDS

Figs 4–10 show (left-hand top panels) close-up schematic finding charts of L35, L45, L49, L50, L62, L63 and L85, respectively. The sizes of the plotting symbols are proportional to the T_1 brightness of the stars. The drawn circles centred on the clusters correspond to $r_{\rm FWHM}$ and $r_{\rm cls}$. In the right-hand top panels, we depict the cluster CMDs for stars distributed within $r < r_{\rm FWHM}$, while right-hand bottom panels present the cleaned cluster CMDs with stars distributed within $r < r_{\rm cls}$. The equal cluster area field CMDs shown in the left-hand bottom panels were used to statistically remove field interlopers in the cluster CMDs.

To statistically clean the cluster CMDs of stars that can potentially belong to the foreground/background fields, we used four circular extractions placed well beyond the cluster ($\gg r_{\rm cls}$) and distributed throughout the observed fields. The four field regions have radii

Table 9. Cluster sizes and field contamination.

Name	Background ($\times 10^4$) (star pixel^{-2})	$r_{\rm FWHM}$ (pixel)	$r_{\rm cls}$ (pixel)	Field contamination (per cent)	
				$r < r_{\rm FWHM}$	$r_{\rm FWHM} < r < r_{\rm cls}$
L35	92.5 ± 1.0	30	60	54	85
L45	61.5 ± 1.0	25	80	51	86
L49	68.8 ± 0.5	30	70	70	76
L50	76.5 ± 0.5	20	60	58	90
L62	107.5 ± 0.5	35	120	67	89
L63	106.0 ± 0.5	15	60	62	92
L85	51.0 ± 1.0	160	240	39	63

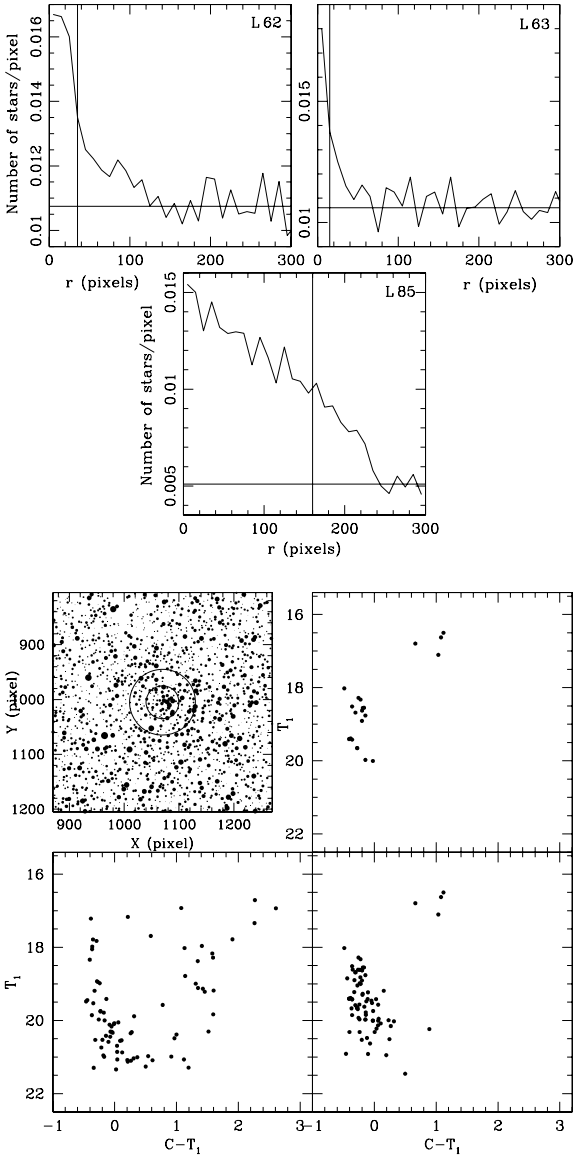

Figure 4. Schematic finding chart of the stars observed in the field of L35 (upper left), with two concentric circles corresponding to $r_{\rm FWHM}$ and $r_{\rm cls}$. North is up and east is to the left. The size of the plotting symbol is proportional to the T_1 brightness of the star. Three extracted CMDs for $r < r_{\rm FWHM}$ (upper right), the cluster surrounding field – normalized to an area of radius $r_{\rm cls}$ – (bottom left) and the cluster cleaned ($r < r_{\rm cls}$) from field contamination (bottom right) are also depicted.

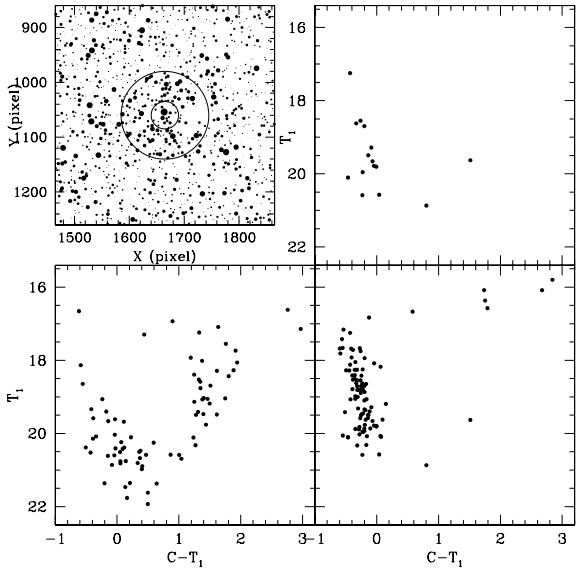

Figure 5. Same as Fig. 2, for L45.

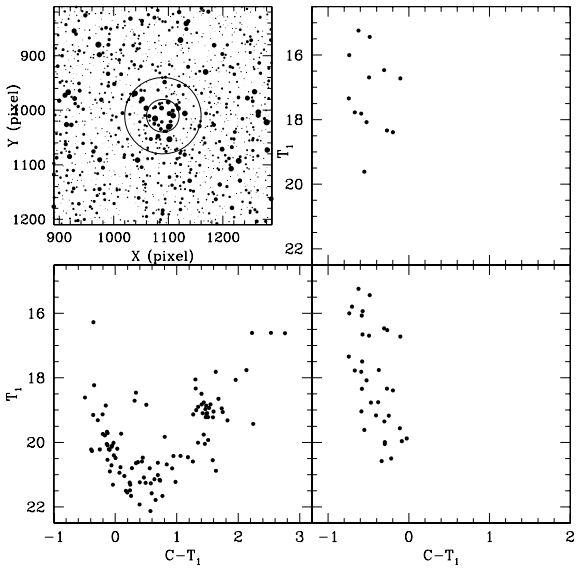

Figure 6. Same as Fig. 2, for L49.

that equal $1/2r_{\rm cls}$, so that the total field comparison area (the sum of these four fields) is equal to that of the cluster area. Using these field CMDs (see left-hand bottom panels of Figs 4–10), we counted how many stars lie in different magnitude–colour bins with sizes $(\Delta T_1, \Delta C - T_1) = (0.5, 0.2)$ mag. We then subtracted from each

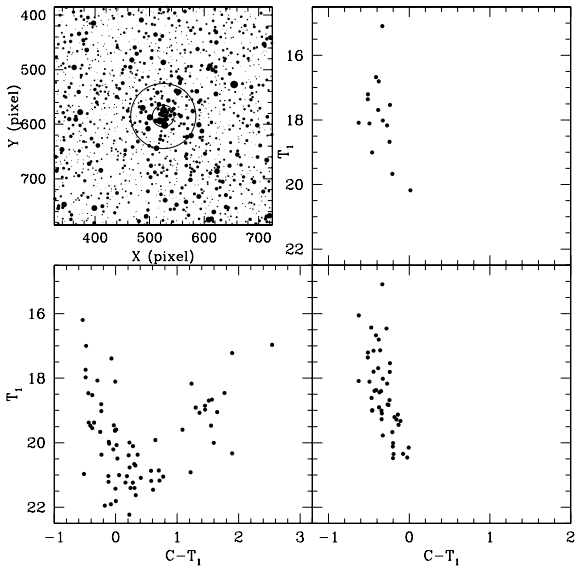

Figure 7. Same as Fig. 2, for L50.

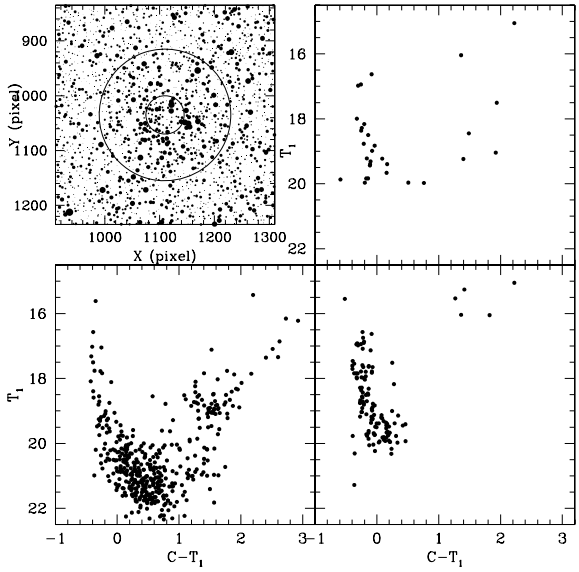

Figure 8. Same as Fig. 2, for L62.

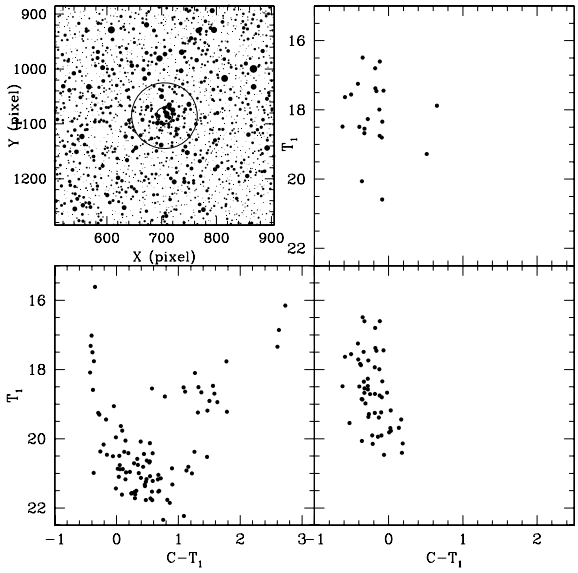

Figure 9. Same as Fig. 2, for L63.

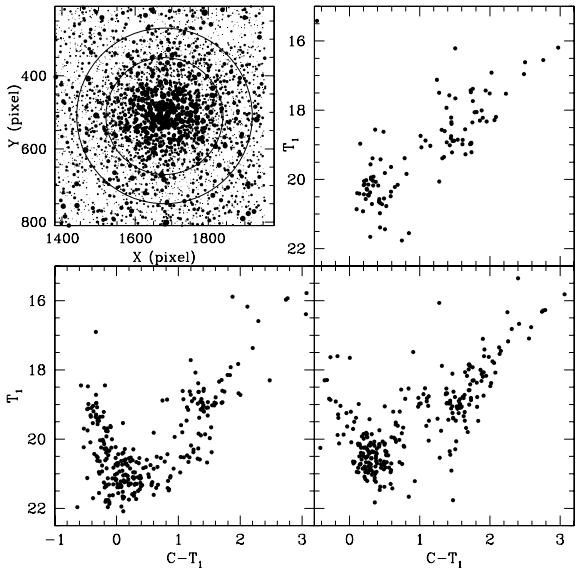

Figure 10. Same as Fig. 2, for L85.

cluster CMD the number of stars counted in the corresponding field CMD in each $(T_1, C - T_1)$ bin, selecting for removal the star closest to that of each field star. In the subsequent analysis, we used the cleaned CMDs for estimating the cluster fundamental parameters, although we kept the CMDs corresponding to the stars within $r_{\rm FWHM}$ as cluster fiducial sequence references. Note that the fiducial MSs of some clusters, although bright, appear somewhat disperse and scattered. This is first due to crowding in the central part of these very small clusters and, secondly, to some unavoidable field interlopers. Other sources of dispersion such as photometric error, differential internal cluster reddening, evolutionary effects or binarity can also take place.

When comparing field and cleaned cluster CMDs, the differences in stellar composition become noticeable, as can be seen when comparing both bottom panels of Figs 4–10. Particularly, the field RC at $T_1 \sim 19$ (which becomes prominent for age $\sim$1–5 Gyr) is the most common field feature, in addition to the field MS composed of stars within a presumably wide age range. L49, L50 and L63 appear to be very young clusters immersed in intermediate-age SMC fields; the upper MS of L49 and L63 showing some trace of evolution. L35, L45 and L62 show some additional evolutionary features typical of clusters several hundred million years old. In L35, a small RC appears at $\sim$16.75. In L45, a few red giants are visible in its outer region. L62 has a RC at $\sim$15.75. Finally, L85 is the most populous cluster of the sample with clear RC and RGB which resemble an intermediate-age star cluster around 1-Gyr old.

In order to estimate the clusters ages, we must take into account that cluster metallicity plays an important role when fitting theoretical isochrones. Indeed, theoretical isochrones with the same age but with different metallicities can range from slightly to remarkably different. The distinction is particularly evident for the evolved phases of the RC and RGB. As far as ZAMSs, they are often less

affected by metallicity effects, and can even exhibit imperceptible variations for a specific metallicity range within the photometric errors. This is the case of the ZAMSs of SMC young- to intermediate-age clusters, of the age range we find for the present cluster sample. Given that all of our clusters are younger than 2 Gyr, the limit for which the Washington SGB technique for deriving metallicity works without significant age correction (Geisler et al. 2003), we must rely on other means to estimate the metallicity. In keeping with our previous work, we have opted to simply assume a representative value of $Z = 0.004$ for SMC clusters in this age range. This is in good agreement with the metallicity generally attributed to the present-day galaxy of ~ -0.65 (e.g. Russell & Bessell 1989; Hill 1997), as well as with the value assumed in the large-scale studies of Pietrzyński et al. (1998) and de Oliveira et al. (2000). We thus used a chemical compositions of $Z = 0.004$ for the isochrone sets varying in steps of $\Delta\log t = 0.05$ dex.

Cluster reddening values were estimated by interpolating the extinction maps of Burstein & Heiles (1982, hereafter BH). BH maps were obtained from H I (21 cm) emission data for the southern sky and provide us with foreground $E(B - V)$ colour excesses which depend on the Galactic coordinates. More recently, Schlegel, Finkbeiner & Davis (1998, hereafter SFD) obtained full-sky maps from 100-μm dust emission. They found that at high latitudes, the dust map correlates well with maps of H I emission, but deviations are coherent in the sky and are especially conspicuous in regions of saturation of H I emission towards denser clouds and of formation of H_2 in molecular clouds. Since the $E(B-V)_{\rm SFD}$ values for our clusters are on average five times higher than the $E(B-V)_{\rm BH}$ values, the SFD values are assumed to be saturated and we used the BH values for these inner SMC clusters. We thus assume only Galactic foreground reddenings which do not allow for any reddening intrinsic to the SMC. Even still, the average of the derived BH values is 0.05 ± 0.02, while the typical reddening estimated by SFD for the SMC is 0.037. Table 10 lists the adopted $E(B-V)$ colour excesses. Note that Pietrzyński & Udalski (1999) derive reddenings for four clusters of our sample. Their $E(B - V)$ values are L35: 0.07, L62: 0.07, L63: 0.06 and L85: 0.04. Except for L35, the values are very close to those from BH, lending confidence to our choice.

As for the cluster distance moduli, we adopt for all the clusters the value of the SMC distance modulus $(m - M)_{\rm o} = 18.77 \pm 0.06$ obtained by Crowl et al. (2001). They also found that, considering BH reddening values for populous SMC clusters, the line-of-sight depth of the galaxy is approximately 6 kpc. Then, bearing in mind that any cluster of the sample could be placed in front of or behind the main body of the SMC, we conclude that the difference in apparent distance modulus could be as large as $\Delta(V - M_V) \sim 0.2$ mag, if a value of 60 kpc is adopted for the mean SMC distance. Given that we estimate an uncertainty of 0.2–0.3 mag in adjusting the isochrones to the cluster CMDs in magnitude, our simple assumption of adopting a unique value for the distance modulus for all of the clusters should not dominate the error budget in our final results. In fact, when overplotting the ZAMS on the observed cluster CMDs, previously shifted by the $E(B - V)$ of Table 10 and $(m - M)_{\rm o} = 18.77$, we generally find an excellent match.

We profited from the available theoretical isochrones computed for the Washington photometric system to estimate age of the clusters. Particularly, we used the isochrones calculated with core overshooting included by the Padova group (Girardi et al. 2002) which lead to results similar to those derived from the Geneva group's isochrones (Lejeune & Schaerer 2001). However, the former reach fainter luminosities, allowing a better fit to the fainter portions of the MS.

Table 10. Fundamental parameters of SMC clusters.

Name	$E(B-V)$ (mag)	Age (Myr)	[Fe/H]	a (°)
L35	0.02	220^{+60}_{-40}	−0.70	0.77
L45	0.07	140^{+50}_{-40}	−0.70	0.93
L49	0.07	25^{+6}_{-5}	−0.70	0.85
L50	0.07	80^{+20}_{-20}	−0.70	0.74
L62	0.06	125^{+35}_{-25}	−0.70	0.77
L63	0.06	110^{+30}_{-20}	−0.70	0.83
L85	0.03	1200^{+150}_{-150}	−0.55	2.03

We then selected a set of isochrones, along with the equations $E(C - T_1) = 1.97\ E(B - V)$ and $M_{T_1} = T_1 + 0.58\ E(B - V) - (V - M_V)$ (Geisler & Sarajedini 1999), and superimposed them on the cluster CMDs, once they were properly shifted by the corresponding $E(B - V)$ colour excess and SMC apparent distance modulus. In the matching procedure, we commonly employed five different isochrones, ranging from slightly younger to slightly older than the derived cluster age. Finally, we chose the isochrone which best reproduces the cluster main features.

Fig. 11 shows the results of the fittings. For each cluster CMD, we plot the isochrone of the adopted cluster age in solid lines, and two additional isochrones bracketing the derived age in dotted lines. In the case of L85 we plot only one additional isochrone with a different metallicity than that adopted for the cluster (see below). The ages of the bracketing isochrones were estimated by taking

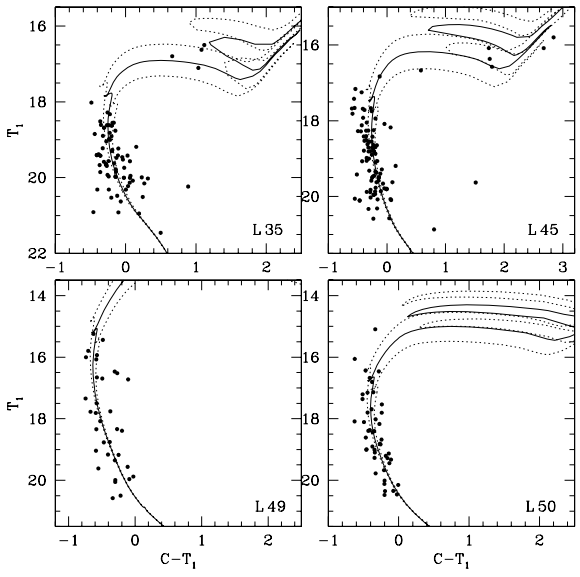

Figure 11. Cleaned Washington T_1 versus $C - T_1$ CMDs for the selected star clusters. Isochrones from Girardi et al. (2002), computed taking into account overshooting are overplotted. The solid and dashed lines correspond to the derived clusters age and to the ages obtained taking into account their associated errors (see columns 3 and 4 of Table 10), respectively: (a) $\log(t) = 8.25$, 8.35 and 8.45 and $Z = 0.004$ for L35 (upper left); $\log(t) = 8.05$, 8.15 and 8.25 and $Z = 0.004$ for L45 (upper right); $\log(t) = 7.30$, 7.40 and 7.50 and $Z = 0.004$ for L49 (bottom left); $\log(t) = 7.80$, 7.90 and 8.00 and $Z = 0.004$ for L50 (bottom right). (b) $\log(t) = 8.00$, 8.10 and 8.20 and $Z = 0.004$ for L62 (upper left); $\log(t) = 7.95$, 8.05 and 8.15 and $Z = 0.004$ for L63 (upper right); $\log(t) = 9.0$ and $Z = 0.008$ and $\log(t) = 9.05$ and $Z = 0.004$ for L85 (bottom).

into account the observed dispersion in the cluster CMDs. The final adopted ages and assumed metallicities for the cluster sample are listed in Table 10.

The presence of RCs and/or RGBs in some cluster CMDs made the fitting procedure easier. We noted, however, that the theoretically computed bluest stage during the He burning core phase are redder than the observed RCs in the CMDs of L35 and L62, a behaviour which has also been detected in other studies of Galactic and Magellanic Cloud clusters (Geisler et al. 2003; Piatti, Clariá & Ahumada 2004a,b, for example). A similar result was found from the fitting of isochrones in the M_V versus $(V-I)_o$ diagram (Piatti, Clariá & Ahumada 2003a,b, among others).

We also derived the age of L85 from the δT_1 index, calculated by determining the difference in the T_1 magnitude of the RC and MS turnoff (TO) in the cluster CMD. We assigned to the TO T_1 magnitude an uncertainty of $\langle\sigma_{TO}\rangle = 0.20$ mag, which is five times that typical of the photometry. Given the crowded nature of this field, the rather sparse RC, and especially the somewhat subjective nature of this procedure, slightly more significant errors may result. Note that this age measurement technique does not require absolute photometry. We then derived the age from $\delta T_1 = 1.00 \pm 0.25$ using equation (4) of Geisler et al. (1997) and this resulted in $t = 1.4 \pm 0.2$ Gyr. Since the TO was measured from the brightest part of the TO region, the age should be considered as a lower limit to the cluster age. Finally, we adopted for L85 an age of $t = 1.2 \pm 0.2$ Gyr, which comes from averaging the δT_1 age and that of the isochrone fitting (see Fig. 11), assigning double weight to the latter.

We then followed the standard SGB procedure of entering absolute M_{T_1} magnitudes and intrinsic $(C-T_1)_o$ colours for this cluster into fig. 4 of Geisler & Sarajedini (1999) to obtain by interpolation the cluster metal abundance [Fe/H]. This derived metallicity is then corrected for age effects via the prescription given in Geisler et al. (2003). We note that ages and metallicities determined in this way have been found to be in good agreement with those derived from comparison to appropriate theoretical isochrones (e.g. Geisler et al. 2003; Piatti et al. 2003a,b). We used the δT_1 age to correct the interpolated metallicity for L85, which led to a final abundance value of [Fe/H] $= -0.55 \pm 0.20$ dex.

5 ANALYSIS AND DISCUSSION

We searched in the literature for previous studies of the present cluster sample. We found only one cluster with a previous metallicity derivation: Kayser et al. (2006) note a value of ~ -0.65 for L85 based on Ca infrared (IR) triplet spectroscopy of a sample of giants. This is pleasingly close to our derived value of -0.55 ± 0.2 for this cluster.

There are a number of studies which have published ages for our clusters. Rich et al. (2000) derived an age of $\sim 2 \pm 0.5$ Gyr for L85 from deep *Hubble Space Telescope* (*HST*) photometry. Kayser et al. note an age for this cluster of ~ 1.2 Gyr, in excellent agreement with our value. From their OGLE photometry, which is roughly equivalent in depth to ours, Pietrzyński & Udalski (1999) found ages of 250, 50, 40 and >1000 for L35, L62, L63 and L85, respectively, assuming $Z = 0.004$, as we do. Chiosi et al. (2006) studied these same clusters together with some 300 other clusters in the context of a discussion of cluster and field star formation in the central part of the SMC. The ages of the clusters were derived from isochrone fitting on to CMDs taken from the same OGLE data base (Udalski et al. 1998). They assumed a distance modulus of $V - M_V = 18.9$ and a mean metallicity of $Z = 0.008$. They also used an interstellar extinction of $E(B-V) = 0.08$, since it was not possible to fit a ZAMS to the four cluster CMDs. Thus, they found ages of 250, 100, 50 and 400 Myr for L35, L62, L63 and L85, respectively. They estimated uncertainties of $\Delta\{\log[t(\mathrm{yr})]\} < 0.3$ for L62 and L63, and >0.5 for L35 and L85. Finally, Rafelski & Zaritsky (2005) derive ages for all of our clusters from the Magellanic Cloud Photometric Survey. They determine ages from their integrated photometry from two different theoretical models. The values (in Myr) they find for our clusters, assuming the same metallicity as we do ($Z = 0.004$), using the Starburst and GALEV models, respectively, are L35: 5 and 100, L45: 10 and 28, L49: 26 and 48, L50: 39 and 108, L62: 4200 and 304, L63: 26 and 28 and L85: 6500 and 2620. Our values are in much better agreement with their GALEV than Starburst ages except for L49. In general, our ages lie within the extremes found from other methods and we will adopt them in the subsequent analysis on the formation history of clusters in the SMC, in particular to maintain consistency with our previous work (e.g. Piatti et al. 2007c).

Mighell, Sarajedini & French (1998, hereafter MSF) estimated the ages – using an age scale where L1 is 9 Gyr – and the metallicities – on the Zinn metallicity scale – of seven old SMC clusters. They also included in their analysis the ages and metallicities of five young SMC clusters discussed in Da Costa & Hatzidimitriou (1998), which represent the present-day properties of the SMC. During the last few years, we have been developing a long-term program consisting in estimating the ages and metallicities of unstudied or poorly studied SMC clusters, based on measurements in the Washington photometric system. These age and metallicity measures rely primarily on the age-calibrated δT_1 index and the isoabundance-calibrated SGBs. Ages and metallicities estimated with these techniques are in the age–metallicity scale of MSF, as pointed out by Piatti et al. (2001, 2007b). For clusters younger than $\sim$1 Gyr, we fitted instead theoretical isochrones to the cluster CT_1 CMDs in order to estimate their ages and assume a metallicity $= -0.7$, since the δT_1 and SGB techniques are not suited and/or calibrated for younger clusters. However, we showed that the derived values are in very good agreement with those obtained from δT_1 and the SGBs for clusters where we used both techniques (Piatti et al. 2002; Geisler et al. 2003), and hence, we can also assume that they are on the same MSF age–metallicity scale. Finally, we also included 11 additional clusters with ages and metallicities derived from integrated spectra (Piatti et al. 2005a), with the aim of enlarging the cluster sample. Piatti et al. (2005a) observed in total 18 clusters, and found that nine of them have ages and metallicities from previous studies in the MSF scale in good agreement with their own estimates.

Table 11 includes all of the clusters with ages and metallicities on this scale, as mentioned above. We distinguish those whose parameters come from the literature, the δT_1 index and the SGBs, the isochrone fitted CT_1 CMDs and the integrated spectra, respectively. Including the seven clusters studied in this paper, they total a sample of 56 clusters.

Such a sample allows us now to investigate the spatial distribution of clusters for different age and metallicity bins, while keeping a statistically reasonable number of objects per bin. In order to trace the cluster formation history and the metallicity enrichment of the SMC, we draw in Fig. 12 the cluster projected positions in the galaxy for four age intervals, namely (t in Gyr): $t > 5$ (upper left-hand panel); $2.5 < t \leq 5$ (upper right-hand panel); $1 < t \leq 2.5$ (bottom left-hand panel) and $t \leq 1$ (bottom right-hand panel), respectively. In each panel, we distinguish in turn four metallicity intervals, namely: [Fe/H] < -1.25 (open triangle); $-1.25 \leq$ [Fe/H] < -1.00 (open square); $-1.00 \leq$ [Fe/H] < -0.6 (open pentagon) and [Fe/H] ≥ -0.6 (open circle), respectively.

Table 11. Ages and metallicities of SMC clusters.

Name	Age (Gyr)	[Fe/H]	Source[a]	Name	Age (Gyr)	[Fe/H]	Source[a]
	Literature				CT_1 isochrones[b]		
L8	6.00	−1.16	1	B 34	1.200	−0.70	5
NGC 121	11.90	−1.71	1	L30	0.160	−0.70	5
NGC 152	1.90	−0.80	2	L34	0.250	−0.70	5
NGC 330	0.025	−0.82	2	L61	0.100	−0.70	5
NGC 339	6.30	−1.50	1	L72	0.025	−0.70	5
NGC 361	8.10	−1.45	1	L106	0.89	−0.70	7
NGC 411	1.50	−0.70	2	L108	0.89	−0.70	7
NGC 416	6.90	−1.44	1	L111	1.00	−0.70	7
NGC 419	1.20	−0.70	2	L114	0.14	−0.70	7
NGC 458	0.13	−0.23	2	L115	0.11	−0.70	7
L1	9.00	−1.35	1				
	δT_1 + SGB				Integrated spectra		
L4	3.10	−0.90	4	L9	1.60	−0.70	8
L5	4.10	−1.20	4	L11	3.50	−1.00	8
L6	3.30	−0.90	4	HW 8	0.05	−0.70[b]	8
L7	2.00	−0.60	4	L37	0.60	−0.70[b]	8
L19	2.10	−0.75	4	L39	0.015	−0.70[b]	8
L27	2.10	−1.30	4	NGC 294	0.32	−0.70[b]	8
L32	4.80	−1.20	3	L51	0.015	−0.70[b]	8
L38	6.00	−1.50	3	L63	0.045	−0.70[b]	8
L43	2.10	−1.13	3	L66	0.015	−0.70[b]	8
L68	3.10	−0.98	3	NGC 422	0.30	−0.70[b]	8
HW 47	2.80	−1.00	4	IC 1641	0.30	−0.70[b]	8
BS 121	2.30	−1.20	4				
HW 84	2.40	−1.20	4				
HW 86	1.60	−0.75	4				
L110	6.40	−1.15	6				
L112	6.70	−1.10	6				
L113	5.30	−1.40	6				

[a](1) MSF; (2) Da Costa & Hatzidimitriou (1998);
(3) Piatti et al. (2001); metallicity recorrected using Geisler et al. (2003);
(4) Piatti et al. (2005b); (5) Piatti et al. (2007a); (6) Piatti et al. (2007b);
(7) Piatti et al. (2007c); (8) Piatti et al. (2005a).
[b]Metallicity adopted.

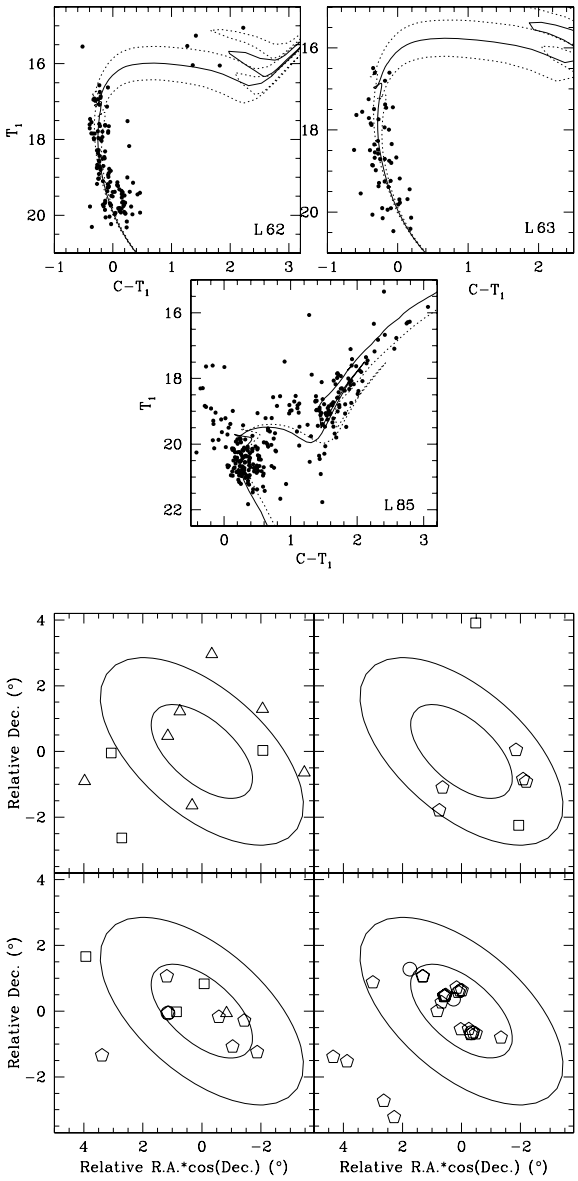

Figure 12. The position of the studied SMC clusters and the 49 clusters from Piatti et al. (2007c) in relation to the SMC optical centre. The semimajor axes of the ellipses drawn in the figure are of 2° and 4°, respectively, and are parallel to the SMC bar. Panels are divided by age (Gyr): $t > 5$ (upper left); $2.5 < t \leq 5$ (upper right); $1 < t \leq 2.5$ (bottom left); $t \leq 1.0$ (bottom right). Symbols represent different metallicity ranges: [Fe/H] < -1.25 (open triangle); $-1.25 \leq$ [Fe/H] < -1.00 (open square); $-1.00 \leq$ [Fe/H] < -0.60 (open pentagon) and [Fe/H] ≥ -0.6 (open circle).

Viewing the SMC as a triaxial galaxy with declination, right ascension and line-of-sight as the three axes, Crowl et al. (2001) found axial ratios of approximately 1:2:4. Based on this result, and with the purpose of describing the spatial distribution of the clusters, we decided to use an elliptical framework following Piatti et al. (2007a) with the SMC major axis aligned with the main bar and a *b*/*a* ratio of 1/2 instead of a spherical framework, in order to reflect more meaningfully the flattening of the galaxy. Thus, the position of the clusters in Fig. 12 are shown relative to the SMC optical centre – assumed to be at $00^{\rm h}52^{\rm m}45^{\rm s}$, $-72^\circ49'43''$ (J2000) (Crowl et al. 2001) – and with two ellipses overplotted with semimajor axes of 2° and 4°, respectively. Finally, note that Fig. 12 allows one to visualize not only the behaviour of the cluster ages and metallicities with distance from the SMC centre but also explore the cluster AMR.

There is a clear trend in Fig. 12, in the sense that the closer a cluster is to the centre of the galaxy, the younger it is, with some dispersion, supporting the results of Noel et al. (2007) who examined the stellar populations of the galaxy from CMDs of 12 star fields located between ∼1° and ∼4° in different parts of the SMC. They also found that intermediate-age and old star populations are distributed throughout the surveyed regions, with a spatial distribution reminiscent of a gradual outside-in formation process. The exceptions to this trend are the four outermost young clusters in the bottom right-hand panel ($t \leq 1$ Gyr), which are associated with the formation process in the Magellanic Bridge region, studied in detail by Harris (2007). The fact that the clusters facing the Magellanic Bridge are younger even in the external region of the SMC is probably due to the interaction with the LMC that has triggered new episodes of star formation.

A weaker tendency is seen in Fig. 12, suggesting that the more metal poor a cluster, the more distant from the SMC centre. Note that in the outer region ($a \geq 4^\circ$) clusters have [Fe/H] ≤ -1.0 with the exception of young clusters associated with the Magellanic

Bridge region, while the inner region is shared by both metal-poor and metal-rich clusters, the average metallicity being clearly larger than that for the outer region. However, all the clusters with [Fe/H] > -1.25 in the inner region were formed during the last 5 Gyr, whereas the metal-poor ones are as old as those in the outer region. Consequently, the abundance gradient seems to reflect the combination of an older and more metal-poor population of clusters spread throughout the SMC and a younger and metal-richer one mainly formed in the inner region. Carrera et al. (2008) studied CaT metallicities of a large number of field giants in each of 12 areas ranging from 1.1° to 3.9° and found evidence for a significant metallicity gradient, which they related with an age gradient in the sense that the youngest stars, which they found to be also the more metal rich, are more concentrated toward the centre of the galaxy, in agreement with our assessment. Finally, note the remarkably different number of clusters in the inner ellipse ($a = 2°$) for ages older and younger than ∼2.5 Gyr. The rapid increase in the number of inner clusters with ages between 2.5 and 1.0 Gyr hints at an important burst of cluster formation, supporting previous results (MSF; Pagel & Tautvaišienė 1998; Rich et al. 2000; Bekki et al. 2004; Chiosi et al. 2006; Piatti et al. 2007c, among others). We note, however, that better cluster statistics are needed to draw more conclusive statements. Finally, note that our results regarding the metallicities of the young clusters are influenced by the fact that we have assumed a metallicity for most of them ($Z = 0.004$) as opposed to deriving our own values.

6 SUMMARY AND CONCLUSIONS

We have used the 1.54-m Danish telescope at the ESO on La Silla to obtain CCD imaging in the Washington system of a number of star clusters in the inner regions of the SMC as part of a continuing project to investigate the cluster formation and chemical evolution history of this important galaxy. Here we have presented the CMDs of L35, L45, L49, L50, L62, L63 and L85. The analysis of the photometric data leads to the following main conclusions.

(i) The observed $(T_1, C - T_1)$ diagrams reveal that there is a high field star contamination in all seven observed fields. To disentangle cluster features from those belonging to their surrounding fields, we traced the cluster stellar density radial profiles to derive the cluster radii. The seven clusters turned out to be relatively small angular sized objects except for L85.

(ii) After a thorough analysis of their radial density profiles, we estimated the percentage of field star contamination as a function of the distance from each cluster's centre. Field star contamination ranges from 40 up to 70 per cent at a distance corresponding to half the maximum of the cluster stellar density profile. The percentage of field stars reaches ∼60–90 per cent at the cluster radius. We then performed a subtraction procedure to statistically clean the cluster CMDs of field star contamination.

(iii) The cleaned CMDs are used to estimate ages for the clusters from a comparison to theoretical isochrones, assuming a metallicity of −0.7. With the exception of L85 which is 1.2-Gyr old, the clusters have ages from 25 up to 220 Myr. These objects increase substantially the sample of clusters in the inner SMC region with well-derived parameters. For L85, we derive a metallicity of -0.55 ± 0.2.

(iv) Combining these results with those for a sample of 49 additional clusters with ages and metallicities put on to the same scale as the present ones, we reinforce previous suggestions with respect to the chemical evolution of the SMC, that the further a cluster is from the centre of the galaxy, the older and more metal poor it is, with some dispersion. This trend is more noticeable for the clusters ages than for their metallicities. Clusters associated with the Magellanic Bridge are clearly an exception, involving young but relatively metal-poor objects.

(v) Independent from the spatial distribution of cluster ages and metallicities and the incompleteness in the cluster sample studied in detail, particularly of clusters younger than 1 Gyr, a bursting cluster formation paradigm – with a burst which occurred at $t \sim 2.5$ Gyr – appears in good agreement with our findings.

ACKNOWLEDGMENTS

This work was partially supported by the Argentinean institutions CONICET and Agencia Nacional de Promoción Científica y Tecnológica (ANPCyT). This work is based on observations made at the ESO. We appreciate the valuable time invested by Luis González obtaining part of the data. We gratefully acknowledge the comments of the reviewer, Emanuela Chiosi, which have improved the manuscript. AS acknowledges support from NSF CAREER grant AST00-94048. DG gratefully acknowledges support from the Chilean *Centro de Astrofísica* FONDAP No. 15010003. CG acknowledges partial support from Chilean CONICYT through FONDECYT grant 1990638 and the Spanish Ministry of Education and Science (grant AYA2004-06343).

REFERENCES

Bekki K., Couch W. J., Beasley M. A., Forbes D. A., Chiba M., Da Costa G. S., 2004, ApJ, 610, L93
Bertelli G., Bressan A., Chiosi C., 1994, A&AS, 106, 275
Burstein D., Heiles C., 1982, AJ, 87, 1165 (BH)
Canterna R., 1976, AJ, 81, 228
Carrera R., Gallart C., Aparicio A., Costa E., Mendez R., Noël N., 2008, AJ, in press (arXiv:0806.4465)
Chiosi E., Vallenari A., Held E. V., Rizzi L., Moretti A., 2006, A&A, 452, 179
Crowl H. H., Sarajedini A., Piatti A. E., Geisler D., Bica E., Clariá J. J., Santos J. F. C., Jr, 2001, AJ, 122, 220
Da Costa G. S., Hatzidimitriou D., 1998, AJ, 115, 1934
de Oliveira M. R., Dutra C. M., Bica E., Dottori H., 2000, A&AS, 146, 57
Gallart C., 1998, ApJ, 495, L43
Geisler D., 1996, AJ, 111, 480
Geisler D., Sarajedini A., 1999, AJ, 117, 308
Geisler D., Bica E., Dottori H., Clariá J. J., Piatti A. E., Santos J. F. C., Jr, 1997, AJ, 114, 1920
Geisler D., Piatti A. E., Bica E., Clariá J. J., 2003, MNRAS, 341, 771
Girardi L., Bertelli G., Bressan A., Chiosi C., Groenewegen M. A. T., Marigo P., Salasnich B., Weiss A., 2002, A&A, 391, 195
Harris J., 2007, ApJ, 658, 345
Hill V., 1997, A&A, 324, 435
Ibata R. A., Lewis G. F., Beaulieu J.-P., 1998, ApJ, 509, L29
Kayser A., Grebel E. K., Harbeck D. R., Cole A. A., Koch A., Gallagher J. S., Da Costa G. S., 2006, preprint (astro-ph/0607047)
King I., 1962, AJ, 67, 471
Kron G. E., 1956, PASP, 68, 125
Lauberts A., 1982, ESO/Uppsala Survey of the ESO (B) Atlas. European Southern Observatory, Garching bei Munchen
Lejeune T., Schaerer D., 2001, A&A, 366, 538
Lindsay E. M., 1958, MNRAS, 118, 172
Mighell K. J., Sarajedini A., French R. S., 1998, AJ, 116, 2395 (MSF)
Noel N. E. D., Gallart C., Costa E., Mendez R. A., 2007, AJ, 133, 2037
Pagel B. E. J., Tautvaišienė G., 1998, MNRAS, 299, 535
Piatti A. E., Geisler D., Bica E., Clariá J. J., Santos J. F. C., Jr, Sarajedini A., Dottori H., 1999, AJ, 118, 2865

Piatti A. E., Santos J. F. C., Jr, Clariá J. J., Bica E., Sarajedini A., Geisler D., 2001, MNRAS, 325, 792
Piatti A. E., Sarajedini A., Geisler D., Bica E., Clariá J. J., 2002, MNRAS, 329, 556
Piatti A. E., Clariá J. J., Ahumada A. V., 2003a, MNRAS, 340, 1249
Piatti A. E., Clariá J. J., Ahumada A. V., 2003b, MNRAS, 346, 390
Piatti A. E., Clariá J. J., Ahumada A. V., 2004a, A&A, 418, 979
Piatti A. E., Clariá J. J., Ahumada A. V., 2004b, A&A, 421, 991
Piatti A. E., Santos J. F. C., Jr, Clariá J. J., Bica E., Ahumada A. V., Parisi M. C., 2005a, A&A, 440, 111
Piatti A. E., Sarajedini A., Geisler D., Seguel J., Clark D., 2005b, MNRAS, 358, 1215
Piatti A. E., Sarajedini A., Geisler D., Clark D., Seguel J., 2007a, MNRAS, 377, 300
Piatti A. E., Sarajedini A., Geisler D., Gallart D., Wischnjewsky M., 2007b, MNRAS, 381, L84
Piatti A. E., Sarajedini A., Geisler D., Gallart D., Wischnjewsky M., 2007c, MNRAS, 382, 1203
Pietrzyński G., Udalski A., 1999, Acta Astron., 49, 157
Pietrzyński G., Udalski A., Kubiak M., Szymański M., Woźniak P., Zebruń K., 1998, Acta Astron., 48, 175
Piskunov A. E., Schilbach E., Kharchenko N. V., Röser S., Scholz R.-D., 2008, A&A, 477, 165
Rafelski M., Zaritsky D., 2005, AJ, 129, 2701
Rich R. M., Shara M., Fall M., Zurek D., 2000, AJ, 119, 197
Russell S. C., Bessell M. S., 1989, ApJS, 70, 865
Schlegel D. J., Finkbeiner D. P., Davis M., 1998, ApJ, 500, 525 (SFD)
Stetson P. B., Davis L. E., Crabtree D. R., 1990, in Jacoby G. H., ed., ASP Conf. Ser. Vol. 8, CCDs in Astronomy. Astron. Soc. Pac., San Francisco, p. 289
Udalski A., Szymaski M., Kubiak M., Pietrzynski G., Wozniak P., Zebrun K., 1998, Acta Astron., 48, 147
Zaritsky D., Lin D. N. C., 1997, AJ, 114, 2545
Zaritsky D., Harris J., Grebel E. K., Thompson I. B., 2002, ApJ, 534, L53

SUPPORTING INFORMATION

Additional Supporting Information may be found in the online version of this article.

Table 2. CCD CT_1 data of stars in the field of L35.
Table 3. CCD CT_1 data of stars in the field of L45.
Table 4. CCD CT_1 data of stars in the field of L49.
Table 5. CCD CT_1 data of stars in the field of L50.
Table 6. CCD CT_1 data of stars in the field of L62.
Table 7. CCD CT_1 data of stars in the field of L63.
Table 8. CCD CT_1 data of stars in the field of L85.

Please note: Blackwell Publishing is not responsible for the content or functionality of any supplementary materials supplied by the authors. Any queries (other than missing material) should be directed to the corresponding author for the article.

This paper has been typeset from a TEX/LATEX file prepared by the author.